36th European Modeling & Simulation Symposium, 025

21th International Multidisciplinary Modeling & Simulation Multiconference

2724-0029 © 2024 The Authors.
doi: 10.46354/i3m.2024.emss.025

Designing a low-energy fiber-optic interconnect link of terabyte throughput for hyper-scale Data Centers

Mikhail E. Belkin[1,*], Evgeny Plastinin[1] and Nikita Smirnov[1]

[1]MIREA – Russian Technological University, Vernadsky av., 78, Moscow, 119454, Russian Federation

[*]Corresponding author. Email address: belkin@mirea.ru

Abstract

The paper addresses the design principles of an interface interconnect link for hyper-scale data processing centers that provides a record throughput of more than 6 Tbps with lowest specific energy consumption of 24 pJ/bit. To implement a line with such high throughput, a new optical transceiver design is proposed, which jointly uses well-known time and spectral multiplexing and relatively new spatial multiplexing based on multi-core optical fiber. Another distinctive feature of the developed link is ultra-low specific energy consumption, which is ensured by the use of a surface-emitting semiconductor laser (VCSEL) in the transmitting path of the optical transceiver, the power consumption of which is an order of magnitude lower compared to the distributed feedback laser typically used in modern telecommunication fiber-optic systems. The possibility of high-quality transmission of digital signals with the declared parameters is confirmed by computer simulation in a widely used environment, as well as by formal calculation.

Keywords: Hyper-scale Data Processing Center; fiber-optic interconnect link of terabyte throughput; computer and formal modeling

1. Introduction

By definition, a data processing center (DPC) is a specialized facility that is a connected system of information technology (IT) and engineering infrastructures, the server and network equipment, which is located in special buildings or rooms connected to external networks, both engineering and telecommunications. In general, it performs the functions of processing, storing and distributing information and is focused on solving business problems by providing information services [1]. The widespread development of DPCs began at the end of the last century and is mainly associated with the commercialization of the Internet, when fast connections to Internet networks were massively required to ensure a wide presence on the global network. At the same time, the rapid growth in the number of Internet users, as well as the need to increase the volume and quality of communication, have led to a demand for consolidation of existing DPCs. The growing need for hardware power led to an increase in energy consumption costs, which even then forced DPC's owners to work on optimizing power supply systems.

The emergence of IT giants in the 21st century, developing their own IT infrastructures, has led to the formation of so-called hyper-scale DPCs with an energy consumption capacity of more than 100 MW, the purpose of which is to provide computing power for leading global players, for example, cloud providers and social networks. This class of DPCs must have a developed network of branches connected by ultra-high-speed interface interconnect links (IIL), and the ability to scale over a wide range. In recent years, the

world has seen a significant development of the network architecture of a hyper-scale DPC, which currently contains up to five internal and external levels connected via IILs, designed on the basis of two terminal optical transceivers (OTC) and a fiber optic link (FOL) connecting them with a length of several meters to several kilometers with a standardized throughput of OTCs from 25 to 400 Gbps. However, the modern development of DPCs dictates an increase of at least an order of magnitude while maintaining or minimally increasing power consumption, which requires a change in technologies and interface standards [2].
Following the trends described above, the paper addresses the design principles of an IIL for hyper-scale DPCs that provides a record throughput of at least 4 Tbps with specific energy consumption of no more than 0.1 nJ/bit.

2. State of the art

The sizes and growth rate of annual traffic of global DPCs [1] at the end of the last decade are illustrated in Figure 1. Providing such huge volumes of data was carried out through the development of DPC. infrastructure, which consisted of both expanding existing and opening new large centers.

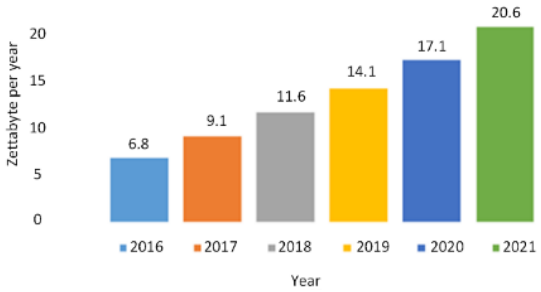

Figure 1. The volume and growth rate of annual traffic of global DPCs

The classification of modern DPCs according to the purpose of the occupied space and, accordingly, power consumption [3] is presented in Table 1.

Table 1. The classification of modern DPCs

Type	Purpose	Square, sq. m	Power consumption, MW
Micro-DPC	Processing IoT data close to the source	for 1 rack	less than 0.01
Low-scale DPC	Enterprise DPC for mission-critical data, production data, and more.	up to 500	up to 1
Average-scale commercial DPC	(including remotely managed services)	up to 10,000	up to 10
Big-scale commercial DPC	Providing DPC space to multiple tenants: individual companies and/or network service providers for the digital ecosystem	up to 50,000	up to 50
Hyper-scale DPC	Computing power for leading global players (e.g. cloud providers and social networks). Sufficient capacity for on-demand scalability.	up to 100,000	more than 100

ABB statistics showing the evolution of the size and energy load of the largest DPCs are illustrated in Table 2 [4, 5], which shows three periods of growth. If the first period (from 1990 to 2000) was characterized by the presence of a DPC with a capacity of up to 2500 racks and a power per rack of about 2 kW, then in the last analyzed period (from 2010 to 2020), it was a DPC of 10,000 racks with an average power per rack ranging from 5 to 17 kW. That is, the last three decades of DPC development have led to a fourfold increase in the volume of its hardware and an average 20-fold increase in energy consumption.

Table 2. Evolution of the size and energy load of the largest data centers over different periods

Area of machine rooms, sq. m	1,500	15,000	30,000	
Number of racks	2,500	5,000	10,000	
Power on one rack, kW	2	4-8	5-17	
Year	1990	2000	2010	2020

The bidirectional IIL studied in the article, connecting two DPCs, has a simple configuration containing two terminal OTC and a FOL connecting them. Since the latter is passive, the total power consumption is entirely determined by the OTCs. State of the art of key parameters for currently produced optical transceivers of O- or C-spectral band are presented in Table. 3. Note that in the "Energy consumption" column, the data in nJ/bit indicated in parentheses, are recalculated for the throughput of this bidirectional IIL

Table 3. The main parameters of currently produced optical transceivers

Model	Producer	Transmission rate, Gbps	Energy consumption,W (nJ/bit)	Line length, km
MMS1C00-C500	Mellanox, USA	100	3,3 (2,64)	up to 2
400G-QSFP-DD-2	Mellanox, USA	400	12 (0,6)	up to 2

DWDM2-Q28100G-80	Arista Networks, USA	100	6,0 (4,8)	up to 80
EOLD-134HG-10-NX6 Series	Eoptolink Technology,USA	400	10 (0,5)	up to 10
EOLD-138HG-5H-SM	Eoptolink Technology,USA	800	12 (0,15)	up to 0,5
AC-QP-3G400-02	LONTE, China China	400	10 (0,5)	up to 2
AC-QP-Q3G400-10	LONTE, China	400	12 (0,6)	up to 10
EOLD-134HG-10-MXX	Eoptolink Technology,USA	400	10 (0,5)	up to 10
EOLD-134HG-02-MXX	Eoptolink Technology,USA	400	10 (0,5)	up to 2
EOLD-854HG-E-02-MXX5 Series	Eoptolink Technology,USA	400	10 (0,5)	up to 0,1

As it follows from the Table, the transmission rate of modern OTCs is predominantly 400 Gbps, and devices with a speed of 800 Gbps are just appearing. However, even this does not meet the needs of modern hyper-scale DPCs. It should also be noted that its increase inevitably leads to an enhance in energy consumption. In order to overcome the above shortcomings, an IIL with an order of magnitude greater throughput and ultra-low specific energy consumption will be described and preliminary investigated below.

3. Conceptual block diagram of the IIL for a hyper-scale DPC

The developed conceptual block diagram of two DPCs interconnected by the IIL, which fundamentally ensures the fulfillment of the above requirements (see Introduction), is shown in Fig. 2. This ultra-high-speed duplex IIL connects two large Data Proceeding Centers of the same level: DPC-1 and DPC-2. Functionally, the IIL includes two terminal OTCs and a fiber-optic cable connecting them.

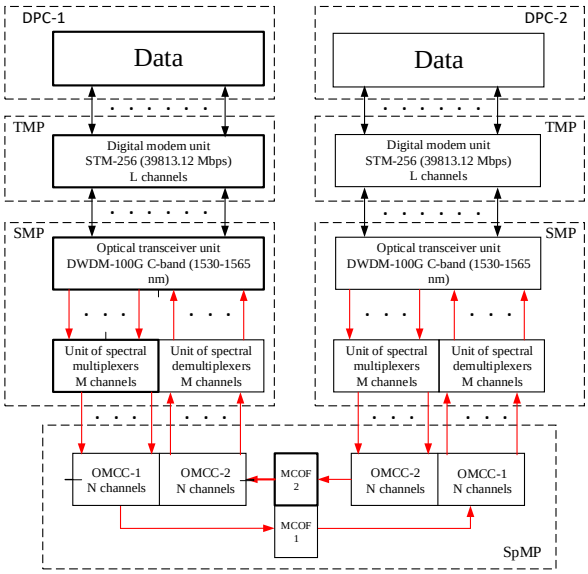

Figure 2. Conceptual block diagram of two DPCs interconnected by the IIL (Black lines are electrical connections, red lines are optical connections)

4. Materials and Methods

According to Figure 2, in the each OTC, the operations of time multiplexing/demultiplexing (TMP or TDMP) and spectral multiplexing/demultiplexing (SMP or SDMP) are sequentially performed. In the fiber-optic link, the operation of spatial multiplexing/demultiplexing (SpMP or SpDMP), the combined use of which fundamentally makes it possible to implement an IIL with a total capacity of 10 and more than what is currently achieved in hyper-scale DPC networks. The implementation of the TMP is carried out using an L-channel digital modem unit, the task of which is to separate or combine digital electrical channels. In practice, this unit can be excluded if communication is carried out not through a single input/output port of each DPC, but directly with its individual hardware racks. The subsequent SMP operation is performed using an M-channel unit of OTCs, containing a set of optical transmitting and photoreceiving devices of the same design based, respectively, on semiconductor laser emitters (SLE) and semiconductor photodetectors (SPD). The frequencies of the optical carriers for the SLE must correspond to the standard DWDM grid in the C-band with a step of 100 GHz [6, 7]. To combine and separate modulated optical signals, M-channel units of spectral multiplexers and demultiplexers are used. The optical transceivers of each data center are connected via a 2-fiber FOL containing N-core multicore optical fibers [8] (MCOF-1 and MCOF-2) terminated with N-pin optical multicore connectors (OMCC-1 and OMCC-2).

In the proposed block diagram, low specific energy consumption is ensured due to:

- relatively low level of TMP (according to preliminary calculations, no more than 40 Gbps);
- use of vertically channel surface emitting lasers (VCSEL) in SMP mode (according to preliminary calculations, 6-8 channels), the power consumption of which is an order of magnitude lower compared to the typically used distributed feedback (DFB) edge emitting laser [9];
- use of passive IIL based on single-mode MCOF [10] (according to preliminary calculations of 7-19 cores).

It is expected that the combined application of the three above approaches will increase the throughput of the IIL to speeds in the petabyte range. At the same time, an important design task is the selection of specific numerical values of L, M and N in order to obtain the optimal ratio between the data transmission rate in each of the L digital electrical channels, the number M of spectral channels and the number N of MSOF cores and the corresponding number of OMCC contacts so as to simultaneously satisfy the specified requirements for throughput and specific energy consumption of the DPC under study, providing the best economic characteristics. A block diagram of one direction of DPC's IIL for further research is presented in Fig. 3.

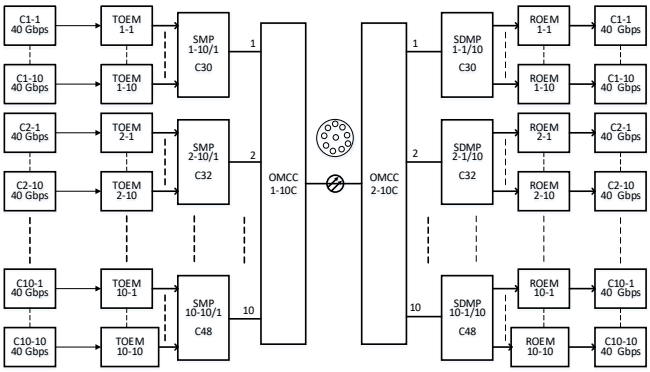

Figure 3. Proposed block diagram of one direction of DPC's IIL

5. The proof-of-concept modeling experiments

Based on the authors' many years of experience in developing the devices of Fig. 3, the initial data for conducting modeling experiments are given in Table. 4.

Table 4. The initial data for modeling experiments

Unit	Device	Parameter	Value
OTC	TOEM/ VCSEL	Spectral range, nm, not more	1540-1555
		Transmitting rate, Gbps, not less	40
		Output optical power, mW, not less	1
		Emission linewidth, MHz, not more	3
		Related intensity noise, dB/Hz, not more	-130
	TOEM/ DFB	Optical carrier tuning, nm, not less	1540-1555
		Output optical power, mW, not less	10
		Emission linewidth, MHz, not more	100
		Related intensity noise, dB/Hz, not more	-150
	SMP/S DMP	Number of spectral channels	8
		Optical loss, dB, not more	1
	ROEM	Spectral range, nm, not less	1546-1553
		Transmitting rate, Gbps, not less	40
		Sensitivity, dBm, not less	-15
		Suppression of spurious channels, dB, not less	80
		Saturation power, dBm, not less	3
IIL	MCOF	Core number	7-19
		Core diameter, μm, not more	9
		Distance between the centers of adjacent cores, μm, not less	30
		Cladding diameter, μm, not more	250
		Optical loss, dB/km, not more	0,5
		Crosstalk, dB, not more	-30
	Total	Throughput, Tbps, not less,	4
		Specific energy consumption, nJ/bit, not more	0,1
		Bit error rate, not more	$1X10^{-11}$

Checking the feasibility of the OTC and IIL parameters specified in Table 4 will be carried out by simulation in the next subsections. A search for computer aided design (CAD) tools showed that there is currently no software that is simultaneously suitable for confirming

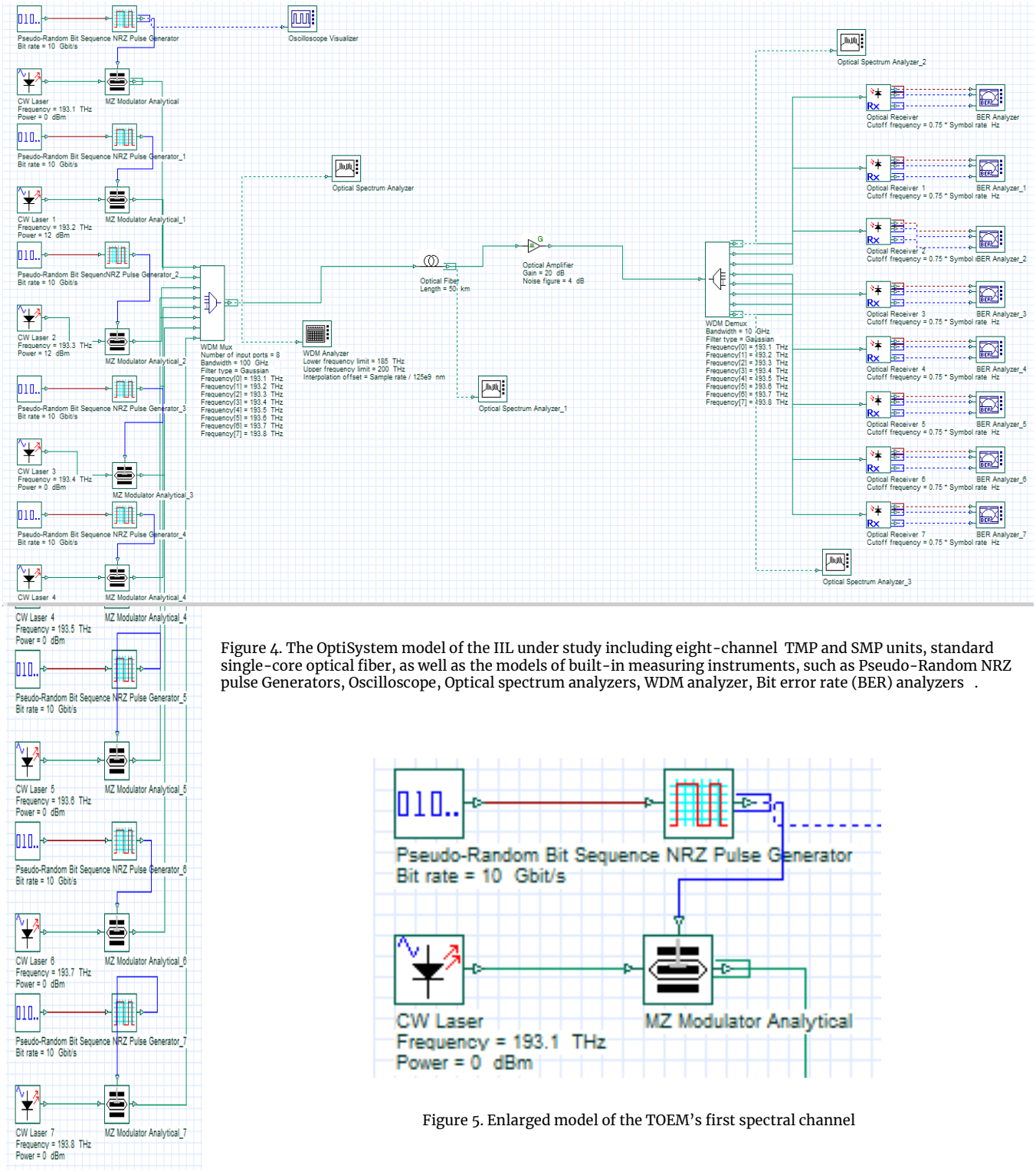

Figure 4. The OptiSystem model of the IIL under study including eight-channel TMP and SMP units, standard single-core optical fiber, as well as the models of built-in measuring instruments, such as Pseudo-Random NRZ pulse Generators, Oscilloscope, Optical spectrum analyzers, WDM analyzer, Bit error rate (BER) analyzers .

Figure 5. Enlarged model of the TOEM's first spectral channel

the correctness of the proposed DPC's IIL scheme of Figure 3 and the feasibility of the numerical initial data of Table 4. Consequently, further consideration will be carried out as follows. First of all, a general simulation of the simplified IIL schematic in the CAD OptiSystem [11] will be performed. Then, using other CADs or by numerical calculation using known formulas, the simulation of the key units of the OTC including the MCOF, will be presented.

5.1. Interface interconnect link

To make the Figure 4 easier to understand, the enlarged model of the TOEM's first spectral channel is presented in Figure 5. As noted above, the remaining TOEM channels of a multi-channel OTC are modeled using a similar scheme with a sequential increase in the frequency of the VCSEL optical carrier by 100 GHz.

Based on the simulations, the following results were obtained. Figure 6 shows the spectrogram of the signal obtained using the built-in model of the optical spectrum analyzer at the output of the transmitting path of the 8-channel OTC (SDMP inputs). In the graph, the horizontal line corresponds to 0 dBm optical output power. As follows from the Figure, the output signal of the OTC contains eight modulated optical signals, the occupied spectrum of which is within the limits specified in Table 4. The distance between adjacent optical carriers corresponds to 0.8 nm. In terms of the frequency range, this amounts to 100 GHz, that is, a standard DWDM signal is observed. However, the output power levels for each spectral channel range from -10 to +4 dBm, that is, their spread is 14 dB. The reason for this scatter is depending on the wavelength of the SLE output power. In the OTC under study, this scatter can be easily compensated by adjusting the gain of the optical amplifier or the power of the master laser. devices, the adjustment of which leads to the possibility of studying the characteristics of the FOL under study. The CAD system used makes it possible to quickly change the parameters inside the simulated FOL, as well as external parameters of the environment to be modeled. In addition, it allows you to simulate both single-channel and multi-channel systems with SMP, such as DWDM and CWDM. The program has the option of working with digital communication systems at information flow rates from 10 Gbps to 300 Gbps. In addition to device modules, there are various monitoring units that allow you to measure key characteristics of the FOL under test, for example, Q-factor, eye diagram, bit error rate (BER), optical spectrum, etc.

OptiSystem is a comprehensive CAD environment that allows to design, simulate and test optical circuits for modern FOLs. This CAD tool has a comprehensive process simulation package, as well as a clear distribution of the components and subsystems used. Active and passive elements have real parameters of the existing optoelectronic, optical and radioelectronic component base.

The OptiSystem model of the IIL under study is shown in Fig. 4. As can be seen from comparison with the block diagram of Fig. 3, due to the lack of the ability to simulate MCOFs in this CAD, it does not contain the models of MSOF unit.

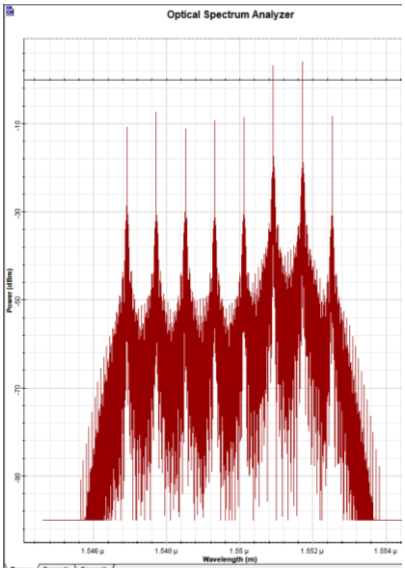

Figure 6. The spectrogram at the output of the OTC transmitting path

In accordance with the diagram in Figure 3, in the receiving path of the OTC, the transmitted group signal is again divided into 8 channels using SDMP, and then converted into the video range using ROEM. Examples of spectra at the output of the SDMP in the first and last channels are shown in Figure 7. As follows from the graphs, the optical power for both channels is about 0 dBm and the suppression of spurious channels is around 90 dB, which corresponds to the data in Table 4.

At the end of the IIL simulation in the OptiSystem CAD system, we calculate the quality of the transmitted signal, which is standardly performed at the output of the OTC according to the criteria of the eye diagram study, Q-factor and bit error rate (BER). The results of calculating these parameters in the first and last OTS channels using standard methods are shown in Figure 8.

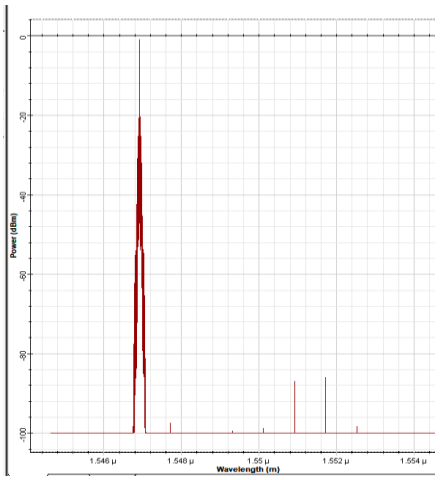

a) Spectrum at the output of the first SDMP channel

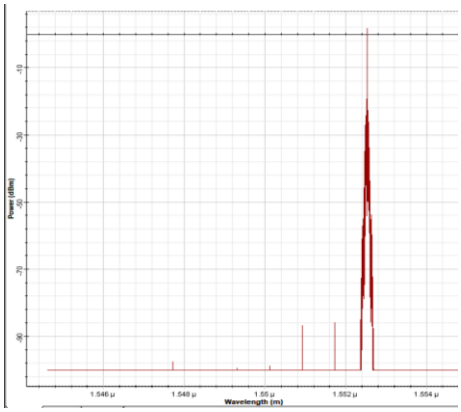

b) Spectrum at the output of the eight SDMP channel

Figure 7. Optical spectra at the output of the SDMP in receiving path of the OTC

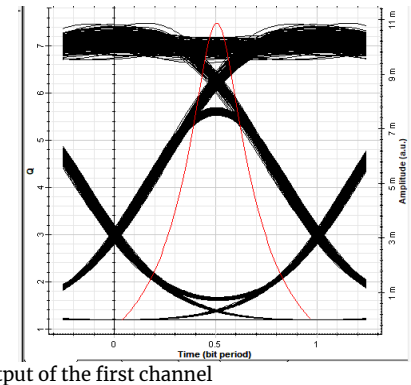

a) At the output of the first channel

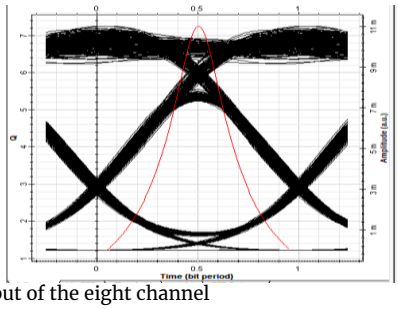

b) At the output of the eight channel

Figure 8. Results of calculating the quality of the transmitted digital signal

As follows from the graphs, the IIL under study provides a sufficiently high quality of the transmitted high-speed digital signal, which is qualitatively confirmed by the openness of both eye diagrams and quantitatively by the fact that the Q-factor is greater than 7 for both channels, and the minimum BER is $3 \cdot 10^{-14}$ for the first channel and $1.7 \cdot 10^{-13}$ on the eighth channel with a standard BER value of no more than $1 \cdot 10^{-11}$ (see Table 4).

5.2. Multicore fiber

In the block diagram shown in Figure 3, the TOEM and ROEM units are connected using a FOL, the key components of which, according to the OptiSystem model of Fig. 4 are a MCOF and a multicore fiber-optic amplifier. The library model of the first component appeared only in the latest version with a very simplified description; the second is still missing, although there are already conference publications describing the results of its success development [12]. Therefore, in order to confirm the correctness and feasibility of the results of developing numerical initial data for modeling in Table 4. below are the mathematical model and results of modeling the transient interference of the MCOF, the use of which is one of the most important topics in this research from the point of view of the novelty of the proposed solution.

5.2.1. Mathematical description

When describing mathematically a transient noise of two waveguides, the Coupled Modes Theory is used. According to it, in axisymmetric optical fibers there is a set of propagating modes. If two such fibers are located close enough, the modes in them will begin to interfere with each other. If the distributions of the electromagnetic field before and after the interaction of the modes do not differ significantly, then the waveguide properties of such fibers can be considered using perturbation theory [13]. In it, the interaction between cores n and m of a MCF can be considered as field propagation in a double-core fiber made up of these cores (Fig. 9). This model assumes the absence of

nonlinear effects associated with quartz glass. In addition, neglecting the effect of birefringence, we can assume that the polarization in both cores is the same, and the interaction occurs only between modes that are non-orthogonal in polarization. Then, the complex amplitude of the propagating electric field can be described as [13, 14]:

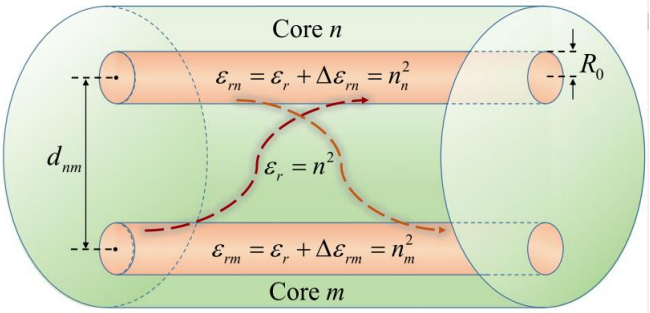

Figure 9. Diagram of a double-core light guide

$$\vec{E}_g(\vec{r}) \approx \vec{E}_n(\vec{r}) + \vec{E}_m(\vec{r}) = \begin{bmatrix} A_n(z) F_n(r,\varphi) \exp(-j\beta_n z) \\ +A_m(z) F_m(r,\varphi) \exp(-j\beta_m z) \end{bmatrix} \cdot \hat{\tau} \quad (1),$$

where $A_{n(m)}$ – complex envelope; $F_{n((m)}$ – distribution of the LP_{01} mode field in the core and cladding; $\beta_{n(m)}$ is the propagation constant of the LP_{01} mode for the case of an unperturbed fiber; $\hat{\tau}$ – unit polarization vector. Let's substitute into Maxwell's equations:

$$\Delta\vec{E}_g(\vec{r}) + k_0^2 \left[\varepsilon_{\mathrm{rg}}(\vec{r})\right] \vec{E}_g(\vec{r}) = \vec{0} \quad (2),$$

where ε_{rg} is the relative electrical permittivity.

$$\varepsilon_{\mathrm{rg}}(\vec{r}) := \varepsilon_r(\vec{r}) + \Delta\varepsilon_{\mathrm{rn}}(\vec{r}) + \Delta\varepsilon_{\mathrm{rm}}(\vec{r}) \quad (3)$$

In addition, for each core the Helmholtz equation must be satisfied:

$$\Delta_T F_{n(m)} + k_0^2 \varepsilon_{\mathrm{rg}} F_{n(m)} = \left[k_0^2 \Delta\varepsilon_{\mathrm{rm}(n)} + \beta_{n(m)}^2\right] F_{n(m)} \quad (4)$$

Combining all expressions, we get:

$$j\left[\frac{dA_n}{dz} + \chi_{\mathrm{nm}} \exp(-j\Delta\beta_{\mathrm{mn}} z) \frac{dA_m}{dz}\right] = c_n A_n + k_{\mathrm{nm}} \exp(-j\Delta\beta_{\mathrm{mn}} z) A_m \quad (5),$$

where $\Delta\beta_{mn}=\beta_m-\beta_n$; k_{nm} is the coupling coefficient between cores n and m.

$$k_{\mathrm{nm}} = \frac{k_o^2}{2\beta_n} \frac{\iint \Delta\varepsilon_{\mathrm{rn}} F_m F_n dS_\infty}{\iint F_n^2 dS_\infty} = \frac{k_o^2 N A_n^2}{2\beta_n} \frac{\iint F_m F_n dS_n}{\iint F_n^2 dS_\infty} \quad (6).$$

Next, to calculate transient losses, we will use the Coupled Power Theory. This approach is based on the principle of measuring signal power, where the power introduced into one core at the input of a fiber is transferred to and out of neighboring cores. The equation of related powers can be written as [15]:

$$\frac{dP_p}{dz} = \sum_{p \neq q} h_{pq}(z)[P_q(z) - P_p(z)], \quad (7),$$

where P_p, Pq – average signal powers in cores p, q; h_{pq} – power coupling coefficient between cores. In the case of identical cores ($\Delta\beta=0$), solving the coupling equations gives an expression for the power-coupling coefficient [16]:

$$h_{nm} = \frac{2k_{nm}^2 R_b}{\beta_m \Lambda} \quad (8),$$

Taking this into account, crosstalk from the core n to the core m results in:

$$\boldsymbol{XT_{nm} = \tanh(h_{nm} L) = \tanh\left(\frac{2k_{nm}^2 R_b L}{\beta_m \Lambda}\right)},$$

where R_b is the bending radius of the fiber; L – length of the light guide; Λ – distance between the centers of the cores.

The above expression is true for the case of interaction of two cores. If any core has n equivalent neighbors, then the crosstalk induced to this core can be estimated as [16]:

$$\boldsymbol{XT_{worst}[dB] = XT_{nm}[dB] + 10\lg(n)} \quad (9),$$

Finally, a core design with a trench of low-index glass can be used to suppress crosstalk (Figure 10).

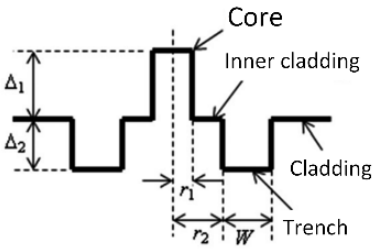

Figure 10. Diagram of a core with a trench of low refractive index glass

Then the crosstalk in such a core can be estimated by knowing the crosstalk in the core without a trench [17]:

$$XT_{trench}[dB] = XT_{step}[dB] + 10\lg\Gamma - 17.4(W_2 - W_1)\frac{W}{r_1}, \quad (10)$$

where $\boldsymbol{\Gamma = W_1/[W_1 + \frac{(W_2-W_1)W}{\Lambda}]}$; $\boldsymbol{W_1 \approx 1.1428V_1 - 0.996}$ for $\boldsymbol{1.5 \le V_1 \le 2.5}$; $\boldsymbol{W_2 = \sqrt{V_2^2 + W_1^2}}$; $\boldsymbol{V_{1(2)} = 2\pi r_1 n_{clad} \frac{\sqrt{2\Delta_{1(2)}}}{\Lambda}}$.

Thus, knowing the distribution of the mode field in each of the cores separately, it is possible to calculate the crosstalk introduced by them in a MCF.

5.2.2. Crosstalk Simulation

As part of crosstalk simulating, a model of a MCF consisting of 19 identical single-mode cores was considered. In development of the Table 4, the

necessary initial data for the calculations are given in Table 5.

Table 5. Main parameters of the MCOF under test

Wavelength, λ	1,55 μm
Cladding refractive index	1,45
Core refractive index	1,4551 (Δ = 0.35%)
Core diameter	9 μm
Cladding diameter	250 μm
Minimum distance between cores, Λ	40 μm
Maximal bend radius, R_b	140 mm
Fiber length, L	5 km

The calculations compared the three most commonly used 19-core MCOF designs: ring, double hexagonal and double ring. Their location diagrams are shown in Fig. 11.

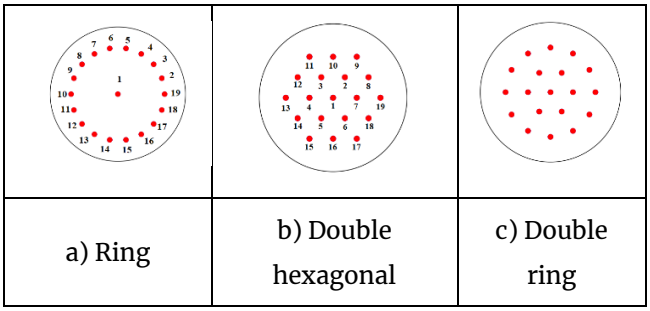

a) Ring | b) Double hexagonal | c) Double ring

Figure 11. Core location diagram in 19-core MCOF under test

To determine the introduced crosstalk, first of all, it is necessary to calculate the mode field distribution of a pair of cores, for which the Comsol Multiphysics software package was used. With its help, the fundamental mode field of each core was first calculated separately, and then the overlap integral between the fields was calculated.

The calculation showed the following results. In the case of a ring core arrangement (Fig. 11a), the largest crosstalk of -13.7 dB is induced between adjacent cores in the outer ring. The disadvantage of this scheme is the small residual thickness of the cladding. So, to level out the effect of fiber micro-bending on losses, it should be at least 30 μm. Also, in the case of a double hexagonal core arrangement (Fig. 11b), the largest crosstalk of -8.9 dB is induced. Unlike the previous scheme, here a large number of cores simultaneously experience significant interference from neighboring ones. For example, six cores affect the central core at once, causing significant interference. However, in this design the residual cladding thickness is greater, which allows the cores to be moved further apart. Finally, in the case of a double ring core arrangement (Fig. 11c), the largest crosstalk of -8.9 dB is induced too. In this design, the greatest crosstalk is induced at the inner ring cores. Compared to the single ring design of Fig. 11a), this one allows for a greater thickness of the outer cladding to be left. Among the disadvantages of such a scheme, it should be noted that there is greater crosstalk on the inner ring of cores than in a double hexagonal scheme.

The results of the study in the form of crosstalk (XT) as a function of the minimum distance between the cores (Λ) for their various configurations (Fig. 11) and internal core design (Fig. 10) are presented in Fig. 12.

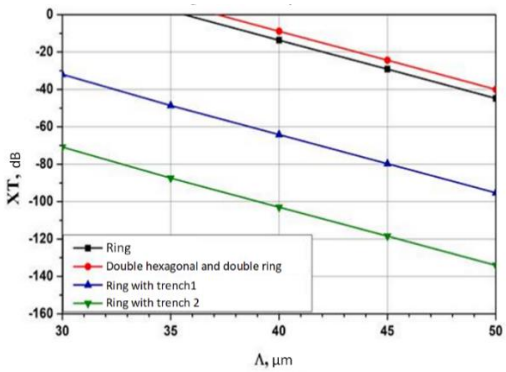

Figure 12. Results of calculating the crosstalk levels.

As the Figure shows, the use of homogeneous cores results in unacceptably high levels of crosstalk in all three configurations. In particular, with a typical core spacing of 40 μm, it exceeds -20 dB, which will lead to a significant deterioration in the quality of transmitted optical signals. An effective way to overcome this situation is to use lower refractive index trenches around the core (see Fig. 10). Namely, depending on the degree of its reduction, the crosstalk level can be reduced to -60 dB or even -100 dB, which will ensure transmission quality at the single-core fiber level.

5.3. Specific energy consumption

To begin with, we will evaluate the full energy consumption of the DPC's IIL for the accepted option for its design. As follows from Figures 2 and 3, its main sources will be OTC's TOEMs and ROEMs. Let us calculate their power consumption, taking a typical efficiency factor of a power supply of 20%. First, we determine the maximum permissible power consumption, which is obtained by multiplying specific energy consumption by the total throughput. As a result, it is 456 W for the circuit in Figure 3. That is, taking into account the efficiency, the maximum power consumed by all OTCs will correspond to 91.2 W. We will accept two options for design an OTC/s TOEM (see Table 4): based on VCSEL (OTC/VCSEL) or DFB laser (OTC/DFB) and the only option for design a ROEM: based on a pin-photodiode and a trans-impedance electronic amplifier. To make the calculations more specific, we will select a typical operating power consumption of 16 mW for a VCSEL, 110 mW for a DFB laser, and 200 mW for a ROEM. In addition, it is necessary to take into account that to adjust the TOEM

frequency using a DWDM grid, a temperature stabilization unit is required, the power of which is 0.1 W for each OTC/VCSEL and 0.2 W for each OTC/DFB. The calculation results are: the total power consumption is 72.0 W for OTC/VCSEL or 107.6 W for OTC/DFB.

Thus, in the case of implementing a TOEMs based on DFB laser, the power consumption significantly exceeds the maximum permissible power of the DPC's IIL under study, that is, the specified energy consumption criterion is not satisfied. On the other hand, it is satisfied with a large margin in the case of using VCSEL, which corresponds to the previously obtained qualitative assumption.

6. Results and Discussion

The results of the simulation showed that the proposed way, based on the joint use of time, spectral and spatial multiplexing, makes it possible to meet the specified requirements for total throughput (at least 4 Tbit/s) and specific energy consumption (no more than 0.1 nJ/bit). In particular, in the proposed interconnect fiber optic link design, a throughput of 6.08 Tbit/s (40 Gbit/s x 8 spectral channels x 19 cores) was obtained with a specific energy consumption of 0.024 nJ/bit, which significantly exceeds the similar parameters of optical transceivers used in interconnecting fiber-optic networks of modern data proceeding centers (see Table 3 for comparison).

7. Conclusions

In this paper, a new system design of a low-energy fiber-optic interconnect link of terabyte throughput for hyper-scale Data Proceeding Centers is proposed and verified by simulation in OptiSystem CAD tool, as well as by formal calculations. Our further work in this topic will be directed to developing the throughput of digital fiber-optic systems up to petabit per second rates.

Funding

This work was funding by Russian Ministry of Higher Education and Science in the framework of grant FSFZ-2022-0005.

References

1. *Cisco Global Cloud Index: Forecast and Methodology, 2016-2021 // Cisco White Paper, (2018)*
2. *Savvas A., et al. "Optical Connections" J., issue 32, p. 10-12 (2023)*
3. *The role of data centers in an interconnected world. - URL: https://withoutyou.de-cix.net/the-role-of data-centers/*
4. *Thiry M. ABB Decathlon® for Data Centers Partner Strategy [Electronic Resource]. - 2021. – URL: https://slideplayer.com/slide/14007994/*
5. *Rack density keeps rising at enterprise data centers [Electronic Resource]. – 2021. – URL: https://datacenterfrontier.com/rack-density-keeps-rising-at-enterprise-data-center*
6. *Recommendation ITU-T G.692*
7. *Schmidt T., Malouin C., Liu S. Recent trends in 100G module and subsystem development for long haul DWDM applications // Optoelectronics and Communications Conference, 2009 / Hong Kong, China. - P. 1-2.*
8. *Zhu B., Taunay T. F., Yan M. F., Fini J. M., Fishteyn M., Monberg E. M., Dimarcello F. V. Seven-core multicore fiber transmissions for passive optical network // Optics Express. - 2010. - No 11. - P. 11117-11122.*
9. *Kapon E., Sirbu A. Long-wavelength VCSELs: Power-efficient answer. // Nature Photonics. - 2009. - T. 3. - № 1. - P. 27-29*
10. *Rosinski B. Chi J.W.D., Grosso P., Le Bihan J. Multichannel Transmission of a Multicore Fiber Coupled with Vertical-Cavity Surface-Emitting Lasers. - M.: J. Lightwave Technol. - 1999. - P. 807-810.*
11. *https://optiwave.com*
12. *Ohtsuka T.*, etc. *Power Efficient Core Pumped Multicore Erbium Doped Optical Fiber Amplifier*. – Optical Fiber Communication (OFC2023) Conference. *San Diego, CA, USA, M1B.4, 3 pp. (2023)*
13. *Okamoto K. Fundamentals of optical waveguides. – Elsevier, 2021.*
14. *Macho A., Morant M., Llorente R. Unified model of linear and nonlinear crosstalk in multi-core fiber //Journal of lightwave technology. – 2016. – T. 34. – №. 13. – C. 3035-3046.*
15. *Koshiba M. et al. Multi-core fiber design and analysis: coupled-mode theory and coupled-power theory //Optics express. – 2011. – V.. 19. – No. 26. – P. B102-B111.*
16. *Saitoh K., Matsuo S. Multicore fiber technology //Journal of Lightwave Technology. – 2016. – V. 34. – No. 1. – P. 55-66.*
17. *Ye F. et al. Simple analytical expression for crosstalk estimation in homogeneous trench-assisted multi-core fibers //Optics express. – 2014. – V. 22. – No. 19. – P. 23007-23018*